Monthly Notices
of the
ROYAL ASTRONOMICAL SOCIETY

MNRAS **448,** 994–1006 (2015) doi:10.1093/mnras/stv025

Formation of a disc gap induced by a planet: effect of the deviation from Keplerian disc rotation

K. D. Kanagawa,[1]★ H. Tanaka,[1] T. Muto,[2] T. Tanigawa[3] and T. Takeuchi[4]

[1]*Institute of Low Temperature Science, Hokkaido University, Sapporo 060-0819, Japan*
[2]*Division of Liberal Arts, Kogakuin University, 1-24-2, Nishi-Shinjuku, Shinjuku-ku, Tokyo 163-8677, Japan*
[3]*School of Medicine, University of Occupational and Environmental Health, Yahatanishi-ku, Kitakyushu, Fukuoka 807-8555, Japan*
[4]*Department of Earth and Planetary Sciences, Tokyo Institute of Technology, Meguro-ku, Tokyo 152-8551, Japan*

Accepted 2015 January 6. Received 2015 January 6; in original form 2014 June 2

ABSTRACT

The gap formation induced by a giant planet is important in the evolution of the planet and the protoplanetary disc. We examine the gap formation by a planet with a new formulation of one-dimensional viscous discs which takes into account the deviation from Keplerian disc rotation due to the steep gradient of the surface density. This formulation enables us to naturally include the Rayleigh stable condition for the disc rotation. It is found that the derivation from Keplerian disc rotation promotes the radial angular momentum transfer and makes the gap shallower than in the Keplerian case. For deep gaps, this shallowing effect becomes significant due to the Rayleigh condition. In our model, we also take into account the propagation of the density waves excited by the planet, which widens the range of the angular momentum deposition to the disc. The effect of the wave propagation makes the gap wider and shallower than the case with instantaneous wave damping. With these shallowing effects, our one-dimensional gap model is consistent with the recent hydrodynamic simulations.

Key words: accretion, accretion discs – planets and satellites: formation – protoplanetary discs.

1 INTRODUCTION

A planet in a protoplanetary disc gravitationally interacts with the disc and exerts a torque on it. The torque exerted by the planet dispels the surrounding gas and forms a disc gap along the orbit of the planet (Lin & Papaloizou 1979; Goldreich & Tremaine 1980). However, a gas flow into the gap is also caused by viscous diffusion and hence the gap depth is determined by the balance between the planetary torque and the viscous diffusion. Accordingly, only a large planet can create a deep gap (Lin & Papaloizou 1993; Takeuchi, Miyama & Lin 1996; Ward 1997; Rafikov 2002; Crida, Morbidelli & Masset 2006).

The gap formation strongly influences the evolution of both the planet and the protoplanetary disc in various ways. For example, a deep gap prevents disc gas from accreting on to the planet and slows down the planet growth (D'Angelo, Henning & Kley 2002; Bate et al. 2003; Tanigawa & Ikoma 2007), and also changes the planetary migration from the type I to the slower type II (Lin & Papaloizou 1986; Ward 1997). Furthermore, a sufficiently deep gap inhibits gas flow across the gap (Artymowicz & Lubow 1996; Kley 1999; Lubow, Seibert & Artymowicz 1999), which is a possible mechanism for forming an inner hole in the disc (Dodson-Robinson & Salyk 2011; Zhu et al. 2011).

Because of their importance, disc gaps induced by planets have been studied by many authors, using simple one-dimensional disc models (e.g. Takeuchi et al. 1996; Ward 1997; Crida et al. 2006; Lubow & D'Angelo 2006) and numerical hydrodynamic simulations (Artymowicz & Lubow 1994; Kley 1999; Varnière, Quillen & Frank 2004; Duffell & MacFadyen 2013; Fung, Shi & Chiang 2014). One-dimensional disc models predict an exponential dependence of the gap depth. That is, the minimum surface density at the gap bottom is proportional to $\exp[-A(M_{\rm p}/M_*)^2]$, where $M_{\rm p}$ and M_* are the masses of the planet and the central star, and A is a non-dimensional parameter (see also equation 38). On the other hand, recent high-resolution hydrodynamic simulations done by Duffell & MacFadyen (2013, hereafter DM13) show that the gap is much shallower for a massive planet than the prediction of one-dimensional models. According to their results, the minimum surface density at the gap is proportional to $(M_{\rm p}/M_*)^{-2}$. Varnière et al. (2004) and Fung et al. (2014) obtained similar results from their hydrodynamic simulations. Its origin has not yet been clarified by the one-dimensional disc model. Fung et al. (2014) also estimated the gap depth with a 'zero-dimensional' analytic model, by simply assuming that the planetary gravitational torque is produced only at the gap bottom. Their simple model succeeds in explaining

★ E-mail: kanagawa@lowtem.hokudai.ac.jp

the dependence of the minimum surface density of $\propto (M_{\rm p}/M_*)^{-2}$. However, the zero-dimensional model does not give the radial profile of the surface density (or the width of the gap). It is not well understood what kind of profile accepts their assumption on the planetary torque. Further development of the one-dimensional gap model is required in order to clarify both the gap depth and width. Such a model enables us to connect the gaps observed in protoplanetary discs with the embedded planets.

One of the problems of the one-dimensional disc model is the assumption of the Keplerian rotational speed. The disc rotation deviates from the Keplerian speed due to a radial pressure gradient (Adachi, Hayashi & Nakazawa 1976). When a planet creates a deep gap, the steep surface density gradient increases the deviation of the disc rotation significantly, which affects the angular momentum transfer at the gap (see Sections 2.1 and 2.2). Furthermore, a large deviation of the disc rotation can also violate the Rayleigh stable condition for rotating discs (Chandrasekhar 1939). A violation of the Rayleigh condition promotes the angular momentum transfer and makes the surface density gradient shallower so that the Rayleigh condition is only marginally satisfied (Tanigawa & Ikoma 2007; Yang & Menou 2010). To examine such feedback on the surface density gradient, we should naturally include the deviation from the Keplerian disc rotation in the one-dimensional disc model.

Another simplification is in the wave propagation at the disc–planet interaction. The density waves excited by planets radially propagate in the disc and the angular momenta of the waves are deposited on the disc by damping. This angular momentum deposition is the direct cause of the gap formation. Most previous studies simply assume instantaneous damping of the density waves after their excitation (e.g. Ward 1997; Crida et al. 2006). If the wave propagation is taken into account, the angular momentum is deposited in a wider region of the disc, which increases the width of the gap (Takeuchi et al. 1996; Rafikov 2002). In a wide gap, the disc–planet interaction would be weak because the disc gas around the planet decreases over a wide region. Hence, we cannot neglect the effect of wave propagation on the gap formation.

In this paper, we re-examine the gap formation by a planet with the one-dimensional disc model, taking into account the deviation from Keplerian rotation and the effect of wave propagation. To include the deviation from Keplerian disc rotation, we modify the basic equations for one-dimensional accretion discs, detailed in the next section. The effect of the wave propagation is included using a simple model. In Section 3, we obtain estimates of gap depths for two simple cases. One estimate for a wide gap corresponds to the zero-dimensional model proposed by Fung et al. (2014). In Sections 4 and 5, we present numerical solutions of the gap without and with wave propagation, respectively. We find that the gap becomes shallow due to the effects of the deviation from Keplerian rotation, the violation of the Rayleigh condition and the wave propagation. With these shallowing effects, our results are consistent with the recent hydrodynamic simulations. In Section 6, we summarize and discuss our results.

2 MODEL AND BASIC EQUATIONS

We examine an axisymmetric gap in the disc surface density around a planet by using the one-dimensional model of viscous accretion discs. Although the Keplerian angular velocity is assumed in most previous studies, we take into account a deviation from Keplerian disc rotation in our one-dimensional model. The deviation cannot be neglected for a deep gap, as will be shown below. We also assume non-self-gravitating and geometrical thin discs. For simplicity, the planet is assumed to be in a circular orbit. We also adopt simple models for density wave excitation and damping to describe the gap formation.

2.1 Angular velocity of a protoplanetary disc with a gap

The angular velocity, Ω, of a gaseous disc around a central star with mass M_* is determined by the balance of radial forces:

$$\Omega^2 R - \frac{GM_*}{R^2} - \frac{1}{\Sigma}\frac{\partial P_{\rm 2D}}{\partial R} = 0, \tag{1}$$

where R is the radial distance from the central star, Σ is the surface density of the disc and $P_{\rm 2D}$ denotes the vertically averaged pressure. On the left-hand side of equation (1), the first term represents the centrifugal force on a unit mass of the disc. The second and third terms are the gravitational force by the central star and the force of the radial pressure gradient, respectively. For $P_{\rm 2D}$, we adopt the simple equation of state $P_{\rm 2D} = c^2\Sigma$, where c is the isothermal sound speed. Using this equation of state, equation (1) can be rewritten as

$$\Omega^2 = \Omega_{\rm K}^2 (1 - 2\eta), \tag{2}$$

with

$$\eta = -\frac{h^2}{2R}\left(\frac{\partial \ln \Sigma}{\partial R} + \frac{\partial \ln c^2}{\partial R}\right), \tag{3}$$

where $\Omega_{\rm K} = \sqrt{GM_*/R^3}$ is the Keplerian angular velocity, and $h = c/\Omega_{\rm K}$

For a disc with no gap, the order of magnitude of the non-dimensional parameter η is $\mathrm{O}(h^2/R^2)$ (Adachi et al. 1976), because the term in parentheses in equation (3) is comparable to $\sim 1/R$. On the other hand, if a planet opens a deep gap with a width of $\sim h$, the steep gradient of the surface density increases η to $\mathrm{O}(h/R)$. Hence, it also enhances the deviation of the disc rotation from the Kepler rotation in the deep gap. We neglect the term $\partial c/\partial R$ in equation (3) because the temperature gradient would be small. Neglecting the smaller terms of $\mathrm{O}(h/R)$, we approximately obtain $\partial\Omega/\partial R$ as

$$\frac{\partial \Omega}{\partial R} = -\frac{3\Omega_{\rm K}}{2R}\left[1 - \frac{h^2}{3}\frac{\partial^2 \ln \Sigma}{\partial R^2}\right]. \tag{4}$$

Note that the second term in the parentheses is of order unity since $\mathrm{d}^2 \ln \Sigma/\mathrm{d}x^2 \sim 1/h^2$ in a deep gap. Therefore, it is found that $\partial\Omega/\partial R$ is significantly altered from the Keplerian value due to the steep gradient of the surface density, though the deviation of Ω is small ($\sim h/R$). As shown later, this deviation promotes radial viscous transfer of angular momentum and makes a gap shallower.

2.2 Basic equations describing a disc gap around a planet

The equations for conservation of mass and angular momentum are given by

$$\frac{\partial \Sigma}{\partial t} + \frac{1}{2\pi R}\frac{\partial F_{\rm M}}{\partial R} = S_{\rm M}, \tag{5}$$

and

$$\frac{\partial}{\partial t}(\Sigma j) + \frac{1}{2\pi R}\frac{\partial F_{\rm J}}{\partial R} = j S_{\rm M} + \frac{1}{2\pi R}\Lambda_{\rm d}, \tag{6}$$

where $F_{\rm M}$ and $F_{\rm J}$ are the radial fluxes of mass and angular momentum, and $j(= R^2\Omega)$ is the specific angular momentum. In equation (5), the source term $S_{\rm M}$ represents the mass accretion rate

on to a unit surface area of the disc. The accretion of disc gas on to the planet can be included in S_M as a negative term. In equation (6), $\Lambda_d(R)$ represents the deposition rate of the angular momentum from the planet on the ring region with radius R.

To describe the deposition rate Λ_d, we consider the angular momentum transfer from the planet to the disc. This transfer process can be divided into two steps. First, the planet excites a density wave by the gravitational interaction with the disc (e.g. Goldreich & Tremaine 1980). Secondly, the density waves are gradually damped due to the disc viscosity or a non-linear effect (Takeuchi et al. 1996; Goodman & Rafikov 2001). As a result of the wave damping, the angular momenta of the waves are deposited on the disc. If instantaneous wave damping is assumed, the deposition rate Λ_d is determined only by the wave excitation. In Section 2.4.1, we will describe the deposition rate for the case with instantaneous wave damping. In Section 2.4.2, we will give a simple model of Λ_d for the case of gradual wave damping.

The radial angular momentum flux F_J is given by (e.g. Lynden-Bell & Pringle 1974)

$$F_J = jF_M - 2\pi R^3 \nu\Sigma\frac{\partial\Omega}{\partial R}. \tag{7}$$

The first term is the advection transport by the disc radial mass flow, F_M, and the second term represents the viscous transport. For the kinetic viscosity, we adopt the α prescription, i.e. $\nu = \alpha ch$ (Shakura & Sunyaev 1973). Note that F_J does not include the angular momentum transport by the density waves in our formulation.

Equations (5)–(7) describe the time evolution of the three variables Σ, F_M and F_J with the given mass source term S_M, the angular momentum deposition rate from a planet Λ_d and the disc angular velocity Ω. Note that Ω depends on $\partial\Sigma/\partial R$, as in equations (2) and (3).

Next, we consider the disc gap in a steady state ($\partial/\partial t = 0$). The time-scale for the formation of a steady gap is approximately equal to the diffusion time within the gap width, $t_{\rm diff} = h^2/\nu$. For a nominal value of α ($\sim 10^{-3}$), the diffusion time is roughly given by 10^3 Keplerian periods, which is shorter than the growth time of planets (10^{5-7} yr; Kokubo & Ida 2000, 2002) or the lifetime of protoplanetary discs (10^{6-7} yr; Haisch, Lada & Lada 2001). Hence, the assumption of a steady gap would be valid. In addition, we assume $S_M = 0$ for simplicity. Although gas accretion on to the planet occurs for $M_p \gtrsim 10\,M_\oplus$ (Mizuno 1980; Kanagawa & Fujimoto 2013), the assumption of $S_M = 0$ would be valid if the accretion rate on to the planet is smaller than the radial disc accretion rate, F_M.

Under these assumptions, equation (5) shows that F_M is constant. Equation (6) yields

$$F_J = F_J(\infty) - \int_R^\infty \Lambda_d dR', \tag{8}$$

where $F_J(\infty)$ is the angular momentum flux without the planet. From equations (7) and (8), we obtain

$$jF_M - 2\pi R^3\Sigma\nu\frac{d\Omega}{dR} = F_J(\infty) - \int_R^\infty \Lambda_d dR'. \tag{9}$$

Equation (9) with a constant mass accretion rate describes a steady disc gap around a planet for a given Λ_d. Since $d\Omega/dR$ is given by equation (4), equation (9) is the second-order differential–integral equation. Note that equation (9) is derived from equation (6) and indicates the angular momentum conservation.

By differentiating equation (9), we obtain a rather familiar expression for the mass flux:

$$F_M = \left(\frac{dj}{dR}\right)^{-1}\left[\frac{d}{dR}\left(2\pi R_p^3\nu\Sigma\frac{d\Omega}{dR}\right) + \Lambda_d\right]. \tag{10}$$

Note that this expression is valid only for the steady state. In a time-dependent case, equation (10) should include the term $-2\pi R\Sigma(\partial j/\partial t)$ in the parentheses. As a boundary condition, the disc surface density should approach its unperturbed values at both sides of the gap far from the planet.

Here, we also consider the unperturbed surface density. In the unperturbed state, Ω can be replaced by Ω_K, by neglecting the smaller term $O(h^2/R^2)$ (see equations 2 and 3). Furthermore, setting $\Lambda_d = 0$ in equation (9), we obtain the unperturbed surface density Σ_0 as

$$3\pi R^2\nu\Omega_K\Sigma_0(R) = -R^2\Omega_K F_M + F_J(\infty). \tag{11}$$

Thus, Σ_0 is given by

$$\Sigma_0 = -\frac{F_M}{3\pi\nu}\left(1 - \frac{F_J(\infty)}{R^2\Omega_K F_M}\right). \tag{12}$$

This agrees with the well-known solution for steady viscous accretion discs (e.g. Lynden-Bell & Pringle 1974).

2.3 Rayleigh condition

For a deep gap around a large planet, the derivative of the angular velocity deviates significantly from the Keplerian velocity, as shown in Section 2.1. A sufficiently large deviation in Ω violates the so-called Rayleigh stable condition of $dj/dR \geq 0$ (see Chandrasekhar 1961). Such a steep gap is dynamically unstable, which would cause a strong angular momentum transfer, lessening the steepness of the gap. This would make the unstable region marginally stable (i.e. $dj/dR = 0$).

Using equation (4), we give dj/dR as

$$\frac{dj}{dR} = \frac{1}{2}R_p\Omega_{Kp}\left(1 + h_p^2\frac{d^2\ln\Sigma}{dR^2}\right), \tag{13}$$

where the suffix p indicates the value at $R = R_p$; this suffix is also used for other quantities. Hence, using the second-derivative of the surface density, the marginally stable condition $dj/dR = 0$ can be rewritten as (Tanigawa & Ikoma 2007).

$$h_p^2\frac{d^2\ln\Sigma}{dR^2} = -1. \tag{14}$$

Actually, around a sufficiently large planet, equation (9) gives $h_p^2 d^2\ln\Sigma/dR^2 < -1$ in some radial regions. In such unstable regions, we have to use equation (14) instead of equation (9).

The breakdown of equation (9) indicates that the flux F_J of equation (7) cannot transport all of the angular momentum deposited by the planet. In a real system, however, the instability would enhance the angular momentum flux, which keeps the gap marginally stable. The enhancement of F_J can be considered to be due to an effective viscosity $\nu_{\rm eff}$ enhanced by the instability. Since such an effective viscosity restores equation (9), $\nu_{\rm eff}$ in the unstable region is given by

$$\nu_{\rm eff} = \frac{-jF_M + F_J(\infty) - \int_R^\infty \Lambda_d dR'}{4\pi R^2\Sigma\Omega}, \tag{15}$$

where we use the relation $d\Omega/dR = -2\Omega/R$ obtained from the marginally stable condition. Furthermore, by using $\nu_{\rm eff}$ instead of

ν, equation (7) gives the enhanced angular momentum flux in the unstable region.

The Rossby wave instability may be important for the gap formation (e.g. Richard, Barge & Le Dizès 2013; Zhu, Stone & Rafikov 2013; Lin 2014). As well as the Rayleigh condition, the Rossby wave instability relates to the disc rotation (Li et al. 2000). Because it can occur before the Rayleigh condition is violated, however, the Rossby wave instability may suppress the surface density gradient more than the Rayleigh condition. For simplicity, we include only the Rayleigh condition in the present study. A further detail treatment including the Rossby wave instability should be done in future works.

2.4 Angular momentum deposition from a planet

In the disc–planet interaction, a planet excites density waves and the angular momenta of the waves are deposited on the disc through their damping. The angular momentum deposition rate $\Lambda_{\rm d}$ is determined by the later process. First, we will consider the deposition rate $\Lambda_{\rm d}$ in the case with instantaneous wave damping. In this case, the deposition rate is governed only by the wave excitation. Next, taking into account the wave propagation before damping, we will model the deposition rate in a simple form.

2.4.1 Case with instantaneous wave damping

Under the assumption of instantaneous wave damping, the angular momentum deposition rate $\Lambda_{\rm d}(R)$ is equal to the excitation torque density $\Lambda_{\rm ex}(R)$, which is the rate at which a planet adds angular momenta to density waves per unit radial distance at R. That is,

$$\Lambda_{\rm d} = \Lambda_{\rm ex}. \tag{16}$$

At a position far from the planet, the excitation torque density is given by the WKB formula (e.g. Ward 1986) as

$$\Lambda_{\rm ex}^{\rm WKB} = \pm C\pi R_{\rm p}^2 \Sigma \left(\frac{M_{\rm p}}{M_*}\right)^2 \left(R_{\rm p}\Omega_{\rm Kp}\right)^2 \left(\frac{R_{\rm p}}{R-R_{\rm p}}\right)^4, \tag{17}$$

where $C = (2^5/3^4)[2K_0(2/3) + K_1(2/3)]^2/\pi \simeq 0.798$ and K_i denote the modified Bessel functions. The sign of equation (17) is positive for $R > R_{\rm p}$ or negative for $R \leq R_{\rm p}$. In the close vicinity of the planet, $|R - R_{\rm p}| \lesssim h_{\rm p}$, on the other hand, the WKB formula is overestimated. Thus, we model the excitation torque density $\Lambda_{\rm ex}$ with a simple cutoff as

$$\Lambda_{\rm ex} = \begin{cases} \Lambda_{\rm ex}^{\rm WKB} & \text{for} \quad |R-R_{\rm p}| > h_{\rm p}\Delta, \\ 0 & \text{for} \quad |R-R_{\rm p}| \leq h_{\rm p}\Delta. \end{cases} \tag{18}$$

The cutoff length $h_{\rm p}\Delta$ is determined so that the one-sided torque T $(= \int_{R_{\rm p}}^{\infty} \Lambda_{\rm ex} {\rm d}R)$ agrees with the result of the linear theory for realistic discs (Takeuchi & Miyama 1998; Tanaka, Takeuchi & Ward 2002; Muto & Inutsuka 2009). Then, we obtain $\Delta = 1.3$.

Note that the WKB formula is derived for discs with no gap. Petrovich & Rafikov (2012) reported that the torque density is altered by the steep gradient of the surface density because of the shift of the Lindblad resonances. For simplicity, however, we ignore this effect in this paper. Hence, in our model, the excitation torque density $\Lambda_{\rm ex}$ is simply proportional to the disc surface density at R, $\Sigma(R)$, and is independent of the surface density gradient even for deep gaps. For a large planet with a mass of $M_{\rm p}/M_* \gtrsim (h_{\rm p}/R_{\rm p})^3$; furthermore, the non-linear effect would not be negligible for wave excitation (Ward 1997; Miyoshi et al. 1999). This non-linear effect is also neglected in our simple model.

2.4.2 Case with wave propagation

When wave propagation is included, the angular momentum deposition occurs at a different site from the wave excitation and equation (18) is not valid. In this case, the angular momentum deposition is also governed by the damping of the waves. Although the wave damping has been examined in previous studies (e.g. Korycansky & Papaloizou 1996; Takeuchi et al. 1996; Goodman & Rafikov 2001), it is not clear yet how the density waves are damped in a disc with deep gaps. In the present study, therefore, we adopt a simple model of angular momentum deposition, described below.

Since the waves are eventually damped in the disc, the one-sided torque (i.e. the total angular momentum of the waves excited at the outer disc in unit time) is equal to the total deposition rate in the steady state. That is,

$$T = \int_{R_{\rm p}}^{\infty} \Lambda_{\rm ex} {\rm d}R' = \int_{R_{\rm p}}^{\infty} \Lambda_{\rm d} {\rm d}R'. \tag{19}$$

Using the one-sided torque, the angular momentum deposition rate can be expressed by

$$\Lambda_{\rm d} = \pm T f(R), \tag{20}$$

where the distribution function $f(R)$ satisfies $\int_{R_{\rm p}}^{\infty} f(R){\rm d}R = 1$, and the sign is the same as in equation (17). As a simple model, we assume a distribution function $f(R)$ given by

$$f(R) = \begin{cases} \dfrac{1}{w_{\rm d}} & \text{for} \quad x_{\rm d}h_{\rm p} - \dfrac{w_{\rm d}}{2} < |R-R_{\rm p}| < x_{\rm d}h_{\rm p} + \dfrac{w_{\rm d}}{2}, \\ 0 & \text{otherwise.} \end{cases} \tag{21}$$

In this simple model, the non-dimensional parameter $x_{\rm d}$ determines the position of the angular momentum deposition and the parameter $w_{\rm d}$ represents the radial width of the deposition site. The waves propagate from the excitation site to the deposition site around $|x| = x_{\rm d}$. Since the density waves propagate away from the planet, the deposition site is farther from the planet than the excitation site. The parameter $x_{\rm d}$ should be consistent with this condition.

In the case with wave propagation, we use equations (20) and (21) to obtain the gap structure with equation (9). It should be noted that T in equation (20) depends on the surface density distribution through the definition of equation (19), because $\Lambda_{\rm ex}$ is proportional to Σ. These coupled equations are solved as follows. First, we obtain the surface density distribution with equation (9) for a given T. Next, we determine the corresponding mass of the planet from equation (19), using the obtained surface density.

2.5 Local approximation and non-dimensional equations

The typical width of a disc gap is comparable to the disc scaleheight and much smaller than the orbital radius of the planet. Thus, it is convenient to use the local coordinate defined by

$$x = \frac{R - R_{\rm p}}{h_{\rm p}}. \tag{22}$$

Note that the suffix p indicates the value at $R = R_{\rm p}$.

We adopt a local approximation in which terms proportional to $h_{\rm p}/R_{\rm p}$ and higher order terms are neglected. From equations (2) and (3), the deviation in Ω from $\Omega_{\rm K}$ is given by

$$\Omega - \Omega_{\rm K} = \frac{h_{\rm p}\Omega_{\rm Kp}}{2R_{\rm p}} \frac{{\rm d}\ln\Sigma}{{\rm d}x}, \tag{23}$$

and is proportional to h_p/R_p. Thus, the disc angular velocity Ω is replaced by the angular velocity of the planet Ω_{Kp} under the local approximation, and the specific angular momentum j also is given by $R_p^2\Omega_{Kp}$. As for the derivative $d\Omega/dR$, we cannot neglect the deviation from the Keplerian value. Equation (4) yields

$$\frac{d\Omega}{dR} = -\frac{3\Omega_{Kp}}{2R_p}\left(1 - \frac{1}{3}\frac{d^2 \ln \Sigma}{dx^2}\right). \tag{24}$$

Equation (9) can be rewritten in the local approximation as

$$R^2\Omega_{Kp}F_M + 3\pi R_p^2 \nu_p \Sigma \Omega_{Kp}\left(1 - \frac{1}{3}\frac{d^2 \ln \Sigma}{dx^2}\right) = F_J(\infty) - \int_x^\infty \Lambda_d h_p dx'. \tag{25}$$

Because of the local approximation, equation (25) cannot be applied for the wide gap formation. If the half width of gap is narrower than about $1/3R_p$, equation (25) would be valid.

Here, we introduce the non-dimensional surface density, s, defined by

$$s = \frac{\Sigma}{\Sigma_0(R_p)}, \tag{26}$$

where $\Sigma_0(R_p)$ is the unperturbed surface density at $R = R_p$ given by equation (12). Dividing equation (25) by $3\pi R_p^2 \nu_p \Sigma_0(R_p)\Omega_{Kp}$ and using equation (11), we obtain a non-dimensional form:

$$\left(1 - \frac{1}{3}\frac{d^2 \ln s}{dx^2}\right)s = 1 - \frac{1}{3}\int_x^\infty \lambda_d dx', \tag{27}$$

where λ_d is the non-dimensional angular momentum deposition rate defined by

$$\lambda_d = \frac{\Lambda_d h_p}{\pi R_p^2 \nu_p \Sigma_0(R_p)\Omega_{Kp}}. \tag{28}$$

The marginally stable condition can be rewritten as

$$\frac{d^2 \ln s}{dx^2} = -1. \tag{29}$$

This equation is used instead of equation (27) in the Rayleigh unstable region.

The non-dimensional excitation torque density, λ_{ex}, is defined by

$$\lambda_{ex} = \frac{\Lambda_{ex} h_p}{\pi R_p^2 \nu_p \Sigma_0(R_p)\Omega_{Kp}} = \begin{cases} \pm K \dfrac{C}{x^4} s(x) & \text{for } |x| > \Delta, \\ 0 & \text{for } |x| \le \Delta, \end{cases} \tag{30}$$

where the non-dimensional parameter K is given by

$$K = \left(\frac{M_p}{M_*}\right)^2 \left(\frac{R_p}{h_p}\right)^5 \alpha^{-1}. \tag{31}$$

In the above, we use $\nu_p = \alpha h_p^2 \Omega_{Kp}$. In our model, the parameter K is the only parameter that determines the gap structure for the instantaneous damping case.

In the case with instantaneous wave damping, the angular momentum deposition rate is given by $\lambda_d = \lambda_{ex}$ (equation 16). In the case with wave propagation, equation (20) gives

$$\lambda_d(x) = \tilde{T} h_p f(R_p + h_p x), \tag{32}$$

where the non-dimensional one-sided torque, $\tilde{T}$, is given by

$$\tilde{T} = K \int_\Delta^\infty \frac{C}{x^4} s(x) dx. \tag{33}$$

Note that the deposition rate λ_d includes two parameters x_d and w_d, in addition to K. In this case, we solve equation (27) for a given value of $\tilde{T}$. Then, we can obtain K by substituting the solution $s(x)$ into equation (33), as mentioned at the end of the last subsection. In order to obtain the solution for a certain K, we need an iteration of the above procedure with trial values of $\tilde{T}$.

The boundary conditions of equations (27) and (29) are

$$s = 1, \quad \text{at } x = \pm\infty. \tag{34}$$

Under the local approximation, the surface density has a symmetry of $s(x) = s(-x)$, since both the above basic equations and the deposition rate are symmetric.

3 ESTIMATES OF GAP DEPTHS FOR SIMPLE SITUATIONS

3.1 Case of the Keplerian discs

Before deriving the gap solution in our model described in Section 2, we examine the gaps for two simple situations. First, we consider a disc with Keplerian rotation, as assumed in previous studies. Neglecting the deviation in $d\Omega/dR$ from the Keplerian (i.e. the term of $d^2 \ln s/dx^2$) in equation (27), we have

$$s = 1 - \frac{1}{3}\int_x^\infty \lambda_d dx'. \tag{35}$$

Here, we also assume instantaneous wave damping and adopt $\lambda_d = \lambda_{ex}$ (equation 30). Differentiating equation (35), we obtain

$$\frac{d \ln s}{dx} = \begin{cases} \pm \dfrac{C}{3x^4} K & \text{for } |x| > \Delta, \\ 0 & \text{for } |x| \le \Delta. \end{cases} \tag{36}$$

Hence, we obtain the surface density in the Keplerian discs with the instantaneous wave damping as

$$s(x) = \begin{cases} \exp\left(-\dfrac{C}{9|x|^3} K\right) & \text{for } |x| > \Delta, \\ \exp\left(-\dfrac{C}{9\Delta^3} K\right) & \text{for } |x| \le \Delta. \end{cases} \tag{37}$$

Using equation (31), $C = 0.798$ and $\Delta = 1.3$, the minimum surface density, s_{min}, is

$$s_{min} = \exp\left[-0.040\alpha^{-1}\left(\frac{R_p}{h_p}\right)^5 \left(\frac{M_p}{M_*}\right)^2\right]. \tag{38}$$

This solution is almost the same as that in the previous one-dimensional gap model (e.g. Lubow & D'Angelo 2006).

For a very large K, the Rayleigh condition is violated and equations (37) and (38) are invalid. Tanigawa & Ikoma (2007) obtained the gap structure in Keplerian discs, including the Rayleigh condition. Their solution is described in Appendix A. In Appendix B, we also derive gap solutions in Keplerian discs, taking into account the wave propagation with the simple model of equations (20) and (21).

3.2 Case of the wide-limit gap

Next, we consider a situation implied by the zero-dimensional analysis done by Fung et al. (2014), which assumes that the wave excitation occurs only the gap bottom. This assumption would be valid if the gap bottom region is wide enough. Hence, we call this situation 'wide-limit gap' case. Since the density waves are excited

at the gap bottom with $s \simeq s_{\rm min}$, the one-sided torque of equation (33) is simply given by

$$\tilde{T} = \frac{C}{3\Delta^3} K s_{\rm min} \simeq 0.121 K s_{\rm min}. \tag{39}$$

Using equation (27), we can estimate $s_{\rm min}$ of the wide-limit gap. The right-hand side of equation (27) can be rewritten as $1 - \tilde{T}/3$ at $x = 0$. In the left-hand side of equation (27), moreover, we can neglect the term $\mathrm{d}^2 \ln s/\mathrm{d}x^2$ when a flat-bottom gap is assumed. Then, the relation between $s_{\rm min}$ and $\tilde{T}$ is obtained as

$$s_{\rm min} = 1 - \frac{\tilde{T}}{3}. \tag{40}$$

Equations (39) and (40) yield

$$s_{\rm min} = \frac{1}{1 + 0.040K}. \tag{41}$$

For a large K, $s_{\rm min}$ given by equation (41) is proportional to $1/K$. This result agrees with the zero-dimensional model by Fung et al. (2014).[1] In the zero-dimensional model, the minimum surface density is estimated from a balance between the planetary torque and the viscous angular momentum flux outside the gap. Such a balance is also seen from equation (40) (and equation 27). The first and second terms in the right-hand side of equation (40) correspond to the viscous angular momentum flux outside the gap and the planetary torque and the left-hand side is negligibly small for a large K.

With their hydrodynamic simulations for $K \lesssim 10^4$, DM13 derived a similar result,[2]

$$s_{\rm min} = \frac{29}{29 + K} = \frac{1}{1 + 0.034K}. \tag{42}$$

It is found that equations (41) and (42) are consistent with each other. Note that these minimum surface densities are much larger than that of the Keplerian disc (equation 38) for a large K because equation (39) is not accepted in the Keplerian solution. The wide-limit gaps assume that all the waves are excited in the bottom region with $s \simeq s_{\rm min}$, i.e. equation (39). In Sections 4 and 5, we will check whether or not this assumption is valid, by comparing it with our one-dimensional solutions.

4 GAP STRUCTURE IN THE CASE WITH INSTANTANEOUS WAVE DAMPING

4.1 Linear solutions for shallow gaps

Here, we present the numerical solution of the gap in the case with instantaneous wave damping (i.e. $\lambda_{\rm d} = \lambda_{\rm ex}$).

First, we consider the case with a small K in equation (27), in which $\lambda_{\rm d}$ is proportional to K. This case corresponds to a shallow gap around a small planet. Since $|s - 1|$ is small, it is useful to express the solution as

$$s = \exp(Ky), \tag{43}$$

or $s = 1 + Ky$. As seen in the next subsection, the former expression is better for an intermediate K ($\sim$10). Substituting equation (43) into equation (27) with equation (16), we can expand it into a power series of Ky. The first-order terms give the linear equation of y:

$$\frac{\mathrm{d}^2 y}{\mathrm{d}x^2} - 3y = \mp \begin{cases} \dfrac{C}{3|x|^3} & \text{for} \quad |x| > \Delta, \\ \dfrac{C}{3\Delta^3} & \text{otherwise}, \end{cases} \tag{44}$$

where the sign in the right-hand side is negative for $x > 0$ and positive for $x \le 0$. Equation (44) is an inhomogeneous linear differential equation, and can be integrated with the boundary conditions of equation (34). We do not need to take care of the Rayleigh condition in the shallow gaps. A detailed derivation of the linear solution is described in Appendix C.

Fig. 1(a) shows y, which can be converted into the surface density s by equation (43). In these shallow gaps, the gap depth is almost the same as for the Keplerian case, though our model gives a smooth surface density distribution.

Fig. 1(b) shows the derivative of y which is related to $\Delta\Omega$, as

$$\Delta\Omega = \Omega - \Omega_{\rm K} = K \frac{h_{\rm p}\Omega_{\rm Kp}}{2R_{\rm p}} \frac{\mathrm{d}y}{\mathrm{d}x}, \tag{45}$$

using equations (23) and (43). The absolute value of $\Delta\Omega$ attains a maximum at $|x| \simeq 1.5$. The second-order derivative of y gives the shear, $\mathrm{d}\Omega/\mathrm{d}x$, as

$$\frac{\mathrm{d}\Omega}{\mathrm{d}x} = \frac{\mathrm{d}\Omega_{\rm K}}{\mathrm{d}x} \left(1 - \frac{K}{3} \frac{\mathrm{d}^2 y}{\mathrm{d}x^2} \right), \tag{46}$$

as seen from equation (24). At $|x| > 1.5$, the shear motion is enhanced compared to the Keplerian case, because $\mathrm{d}^2 y/\mathrm{d}x^2 < 0$. Since the shear motion causes viscous angular momentum transfer, this enhancement makes the surface density gradient less steep compared with the Keplerian case, as shown in Fig. 1(a).

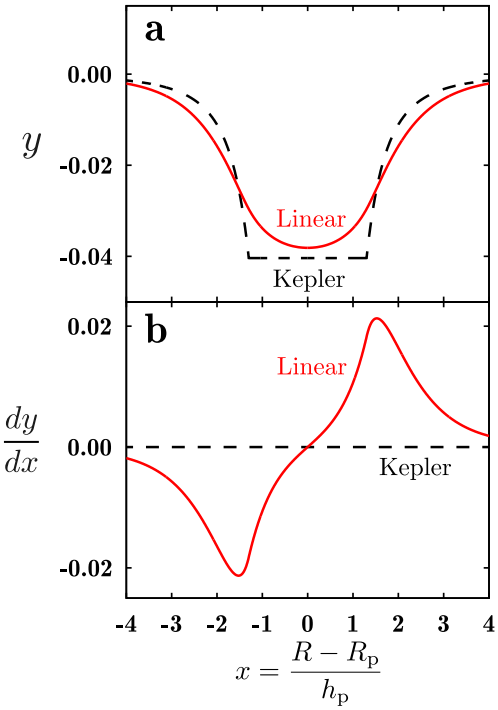

Figure 1. Linear solution for y (a) and $\mathrm{d}y/\mathrm{d}x$ (b). The surface density and angular velocity are given by y and $\mathrm{d}y/\mathrm{d}x$ with equations (43) and (45), respectively. The dashed line is the solution for the Keplerian disc.

[1] In the notation of Fung et al. (2014), K is given by $q^2/(\alpha[h/r]^5)$.
[2] In the notation of DM13, K is given by $\mathcal{M}^{-1}(M_{\rm sh}/M_{\rm p})^2\alpha^{-1}$.

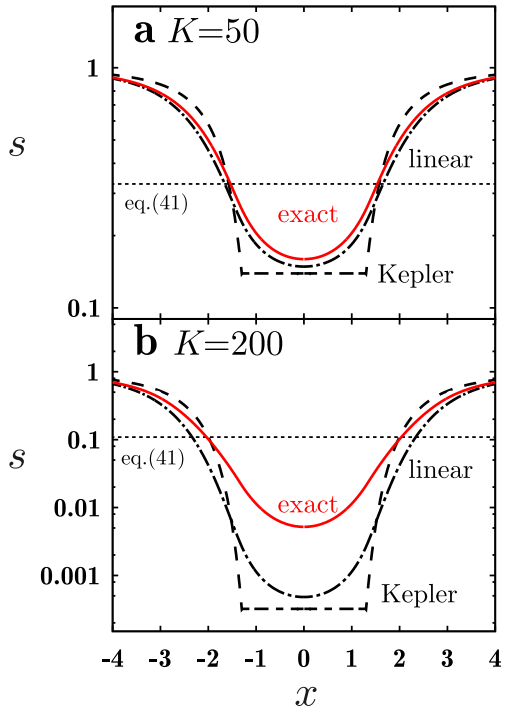

Figure 2. Surface density distributions for $K = 50$ (a) and 200 (b). The red line is the exact solution (see text). The chain line is the linear solution given by equation (43) and the dashed line is the solution for the Keplerian case (equation 37). The dotted line represents the minimum surface densities for the wide-limit gap given by equation (41).

4.2 Non-linear solutions for deep gaps

Next, we consider deep gaps around relatively large planets. In this case, we numerically solve the non-linear equation (27) with the Rayleigh condition. We call the obtained non-linear solution the 'exact' solution.

At regions far from the planet, the surface density perturbation is rather small and the linear approximation is valid. Thus, we adopt a linear solution at $|x| > 10$. Note that this linear solution has different coefficients for the homogeneous terms from those in Section 4.1 (see Appendix C). The coefficients of the homogeneous solution are given to satisfy the boundary conditions of equation (34). At $|x| \leq 10$, we integrate equation (27) with the fourth-order Runge–Kutta integrator. In the Rayleigh unstable region, the surface density is governed by the marginally stable condition (equation 29), instead of equation (27). Fig. 2 shows the surface density distributions of the exact solutions for $K = 50$ (a) and 200 (b). If we assume a disc with $h_p/R_p = 0.05$ and $\alpha = 10^{-3}$, these cases correspond to $M_p = 1/8M_J$ and $1/4M_J$, respectively, where M_J is the mass of Jupiter. For comparisons, the Keplerian solution (equation 37) and the linear solution with equation (43) are also plotted. For $K = 50$, the linear solution almost agrees with the exact solution, while it is much deeper than the exact solution for $K = 200$. For $K = 200$, the Keplerian solution has a much smaller $s_{\rm min}$ than the exact solution. Fig. 3 illustrates the angular velocities (a) and specific angular momenta (b) for the exact solutions for $K = 50$ and 200. Similar to the linear solution in Fig. 1, the shear motion is enhanced at $|x| \gtrsim 1.4$. This enhancement of the shear motion is also seen in Fig. 4. The enhancement promotes the angular momentum transfer and makes the surface density gradient less steep. For $K = 200$, the Rayleigh condition is violated. In the unstable region, the marginally stable condition further reduces the surface density gradient. This

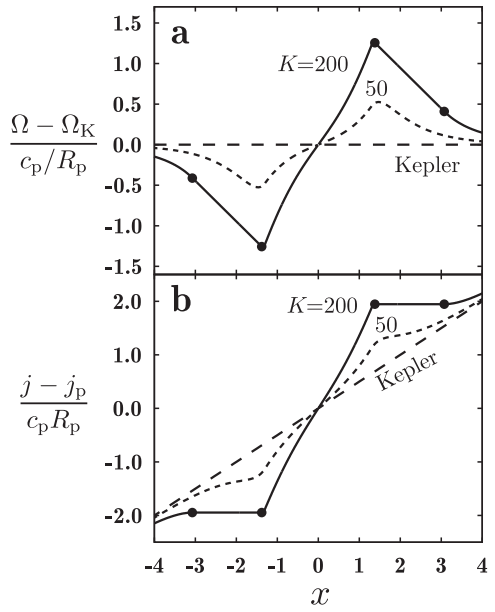

Figure 3. (a) Deviation from Keplerian disc rotation and (b) specific angular momentum, for $K = 50$ (dashed) and 200 (solid). The filled circles indicate the edge of the marginally stable region for the Rayleigh condition.

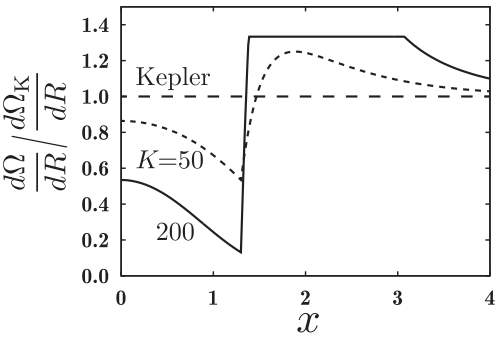

Figure 4. Shear of exact solutions for $K = 50$ (dashed) and 200 (solid).

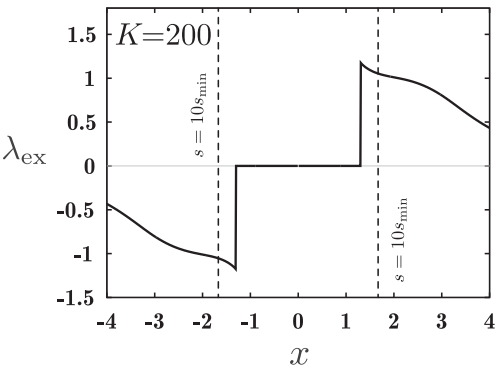

Figure 5. Excitation torque density given by equation (30) for $K = 200$. The two vertical lines indicate the positions with $s = 10s_{\rm min}$.

makes the gap much shallower than for the Keplerian solution, as seen in Fig. 2(b). We also plot the minimum surface densities, $s_{\rm min}$, of the wide-limit gap (equation 41) in Fig. 2. The wide-limit gap gives a much larger $s_{\rm min}$ than the exact solution for $K = 200$. In the wide-limit gap, it is assumed that the density waves are excited only at the gap bottom with $s \simeq s_{\rm min}$. Fig. 5 shows the excitation

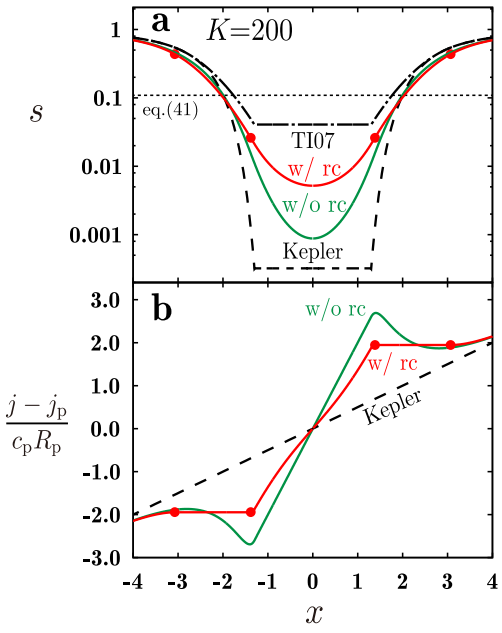

Figure 6. (a) Surface density distribution and (b) specific angular momentum distribution, for $K = 200$. The red line indicates the exact solution. The green line is the solution without the Rayleigh condition (see text). The chain line in (a) denotes the surface density distribution given by the model of TI07(equation A3).

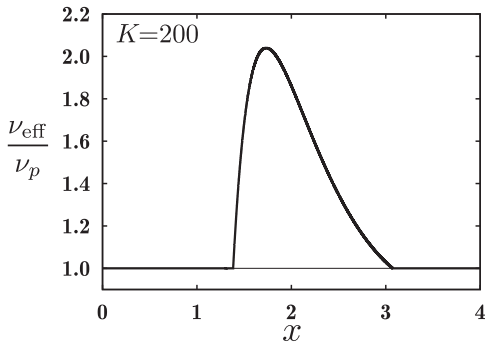

Figure 7. Effective viscosity $\nu_{\rm eff}$ of the exact solution with $K = 200$.

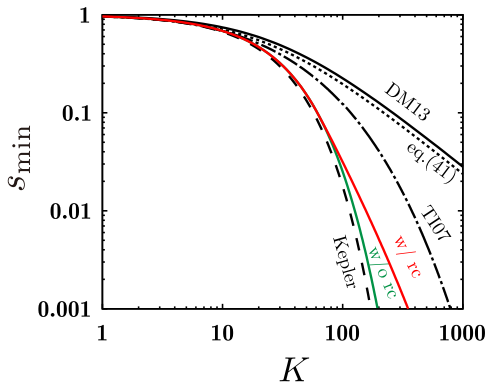

Figure 8. Minimum surface densities, $s_{\rm min}$, for the exact solution (red line) and the solution without the Rayleigh condition (green line). The dashed line is $s_{\rm min}$ in the Keplerian case. The chain, dotted and solid lines denote $s_{\rm min}$ given by the model of TI07, the wide-limit gap (equation 41) and the empirical relation of DM13 (equation 42), respectively.

torque density given by equation (18) for the exact solution with $K = 200$. This torque density indicates that the waves are excited mainly in the region with $s > 10 s_{\rm min}$. Thus, the assumption of wave excitation at the gap bottom is not valid in this case. Since wave excitation with a larger s increases the one-sided torque, this can explain why the gap of the exact solution is much deeper than the wide-limit gap in Fig. 2. Note that this result for the wave excitation is obtained in the case of instantaneous wave damping. The effect of the wave propagation can change the gap width and the mode of wave excitation, as seen in the next section.

4.3 Effect of the Rayleigh condition

We further examine the effect of the Rayleigh condition on the gap structure. Fig. 6 shows the surface densities (a) and specific angular momenta (b) for the exact solution and the solution without the Rayleigh condition. The solution without the Rayleigh condition has unstable regions with $\mathrm{d}j/\mathrm{d}x < 0$ (i.e. $1.4 < |x| < 3.1$). This comparison between these two solutions directly shows how the Rayleigh condition changes the gap structure. The Rayleigh condition increases $s_{\rm min}$ by a factor of 6 for $K = 200$. This is because the marginal condition of $\mathrm{d}^2 \ln s/\mathrm{d}x^2 \geq -1$ keeps the surface density gradient less steep and makes the gap shallow.

It can be considered that the marginally stable state is maintained by $\nu_{\rm eff}$ of equation (15). The non-dimensional form of equation (15) is given by

$$\frac{\nu_{\rm eff}}{\nu} = \frac{3 - \int_x^\infty \lambda_{\rm d} \mathrm{d}x'}{4s}. \tag{47}$$

Fig. 7 shows $\nu_{\rm eff}$ in the unstable region for $K = 200$. The effective viscosity is twice as large as the original value at $x = 1.8$. This enhancement of the effective viscosity causes the shallowing effect in Fig. 6(a).

In Fig. 6(a), we also plot the surface density distribution given by Tanigawa & Ikoma (2007, hereafter TI07), in which the Rayleigh condition is taken into account (for details, see Appendix A). Their model gives a shallower gap than our exact solution. This is because a very steep surface density gradient in the Keplerian solution is suppressed by the Rayleigh condition to a greater extent than in our model.

We also show that the Keplerian solution by TI07 does not satisfy the angular momentum conservation. The Keplerian solution without the Rayleigh condition (equation 37) is derived just from equation (35) (or equation 27), which is originated from equation (9). In this solution, thus, the angular momentum conservation is satisfied. However, when the Rayleigh condition is violated, the marginal stable condition (equation 29) is used instead of equation (37). Because of this, the surface density at the flat-bottom of TI07's solution does not satisfy equation (35) or the angular momentum conservation, either. This violation is resolved in our formulation because our exact solution always satisfies equation (27) outside the Rayleigh unstable region.[3]

4.4 Gap depth

Fig. 8 shows the minimum surface densities, $s_{\rm min}$, as a function of K for the exact solutions. For comparison, we also plot $s_{\rm min}$

[3] By introducing the effective viscosity of equation (47) and multiplying the LHS of equation (27) by $\nu_{\rm eff}/\nu_0$, equation (27) is recovered in the Rayleigh unstable region.

for the solutions without the Rayleigh condition and the Keplerian solutions. These solutions give deeper gaps than the exact solution, similar to the result of Section 4.2. It is found that the shallowing effect due to the Rayleigh condition becomes significant with an increase in K. This is because the Rayleigh condition is violated more strongly for large K.

In Fig. 8, on the other hand, the exact solution is much deeper than DM13's results and the wide-limit gap, though the latter two cases agree well with each other. The model of TI07 also gives much deeper gaps than DM13. These comparisons indicate that in the case with instantaneous wave damping, our exact solution cannot reproduce the hydrodynamic simulations of DM13. This difference in the gap depth from DM13 is likely to be due to the fact that the assumption of the wide-limit gap is not satisfied in the case with instantaneous wave damping (see Fig. 5). In the next section, we will see that the effect of wave propagation widens the gap and makes the assumption of the wide-limit gap valid.

5 EFFECT OF DENSITY WAVE PROPAGATION

In this section, we consider the effect of wave propagation. Wave propagation changes the radial distribution of the angular momentum deposition. A simple model of angular momentum deposition rate altered by wave propagation is described in Section 2.4.2. Using this simple model, we solve equation (27) with the Rayleigh condition in the similar way to the previous section. At the region far from the planet (i.e. $|x| > 10$), we use the linear solution to equation (C1) with $g(x) = 0$ in this case.

5.1 Gap structure for $K = 200$

Fig. 9 illustrates the surface densities (a) and the excitation torque densities (b) of the exact solutions in the case with wave propagation. The angular momenta of the excited waves are deposited around $|x| = x_{\rm d}$ in our model. A large $x_{\rm d}$ indicates a long propagation length between the excitation and the damping. The parameter K is set to 200. For an increasing $x_{\rm d}$, the gap becomes wider and shallower. The gap width is directly governed by the position of the angular momentum deposition. For $x_{\rm d} = 3$ and 4, the gap depths are consistent with the wide-limit gap (and also DM13). For $x_{\rm d} = 4$, the density waves are excited mainly at the bottom region with $s \simeq s_{\rm min}$, as seen in Fig. 9(b). Moreover, for $x_{\rm d} = 3$, a major part of the wave excitation occurs at the bottom. That is, the assumption of the wide-limit gap is almost satisfied for the solutions with $x_{\rm d} = 3$ and 4. This explains why the gap depths are consistent with the wide-limit gap for these large $x_{\rm d}$.

It is also valuable to compare the gap width with hydrodynamic simulations. DM13 performed a simulation for the case of $M_{\rm p} = 1/4M_{\rm J}$ ($2M_{\rm sh}$ in their notation), $\alpha = 10^{-3}$ and $h_{\rm p}/R_{\rm p} = 0.05$. This case corresponds to $K = 200$. In this simulation, they found that the gap width is about $6h_{\rm p}$, assuming that these gap edges are located at the position with $\Sigma = (1/3)\Sigma_0(R_{\rm p})$ (i.e. $s = 1/3$). If we adopt the same definition of the gap edge, the gap widths of our exact solutions with $x_{\rm d} = 3$ and 4 are $6.1h_{\rm p}$ and $7.7h_{\rm p}$, respectively. Hence, if we take into account the wave propagation and adopt $x_{\rm d} = 3$–4, our exact solution can almost reproduce both of the gap width and depth of the hydrodynamic simulations by DM13, for $K = 200$.

It should be also noted that, for $x_{\rm d} = 2$, the wave excitation mainly occurs at $|x| > x_{\rm d}$ (80 per cent of the excitation torques come from this region). However, the deposition site should be farther from the planet than the excitation site because the density waves propagate away from the planet. Thus, the case with $x_{\rm d} = 2$ does not represent a realistic wave propagation. From now on, we judge that our simple model for the wave propagation is valid if more than half of the one-sided torque arises from the excitation at $|x| < x_{\rm d}$. In the case with $x_{\rm d} = 3$ or 4, the excitation at $|x| < x_{\rm d}$ contributes 55 per cent or 78 per cent of the one-sided torque, respectively. In Fig. 10, we check the effect of the width of the deposition site, $w_{\rm d}$, for $x_{\rm d} = 3$ and $K = 200$. It is found that the width $w_{\rm d}$ has only a small influence on the gap structure. We show that the deviation from the Keplerian rotation is also important in the case with wave

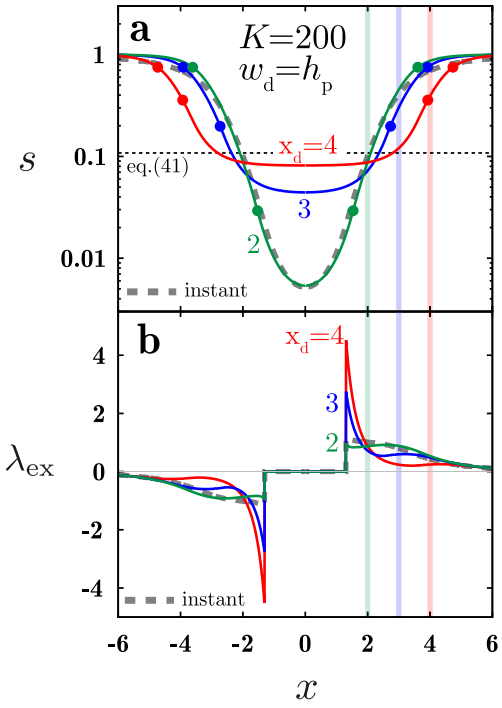

Figure 9. Surface densities (a) and excitation torque densities (b) in the case with the wave propagation for $K = 200$. The green, blue and red lines denote the solutions with $x_{\rm d} = 2$, 3 and 4, respectively. The parameter $w_{\rm d}$ is set to $h_{\rm p}$. The grey dashed line is the surface density in the case with instantaneous wave damping. The dotted line in (a) represents the minimum surface density for the wide-limit gap given by equation (41), i.e. $s_{\rm min} = 0.109$.

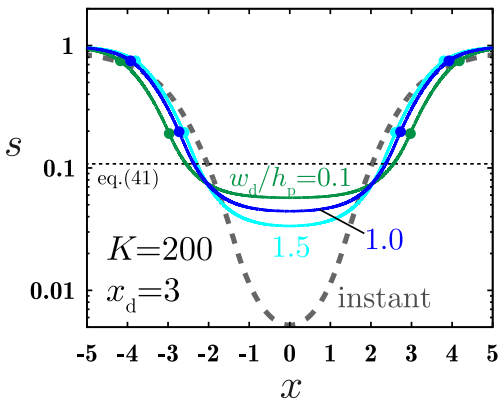

Figure 10. Gap structures for $w_{\rm d} = 0.1h_{\rm p}$ (green), $h_{\rm p}$ (blue) and $1.5h_{\rm p}$ (light-blue). The parameters K and $x_{\rm d}$ are set to 200 and 3, respectively. The grey dashed line indicates the solution in the instantaneous damping case and the dotted line is the minimum surface density of the wide-limit gap (equation 41).

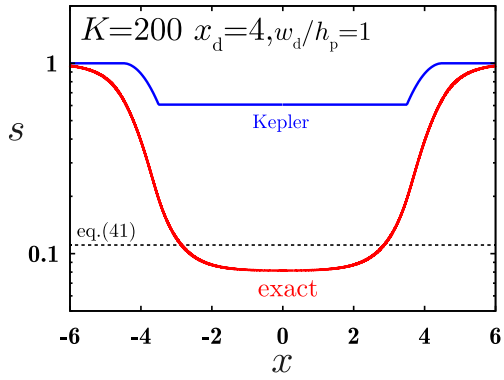

Figure 11. The Keplerian solution in the case of wave propagation for $K = 200$, $x_d = 4$ and $w_d = h_p$ (bule line). For comparison, the exact solution (red line) is also plotted.

propagation. In Fig. 11, we plot the solution with the Keplerian rotation and our exact solution. The Keplerian solution is derived from equation (35) with the angular momentum deposition model (equations 20 and 21). When the Rayleigh condition is violated, the marginal stable condition (equation 29) is used. A detail derivation of this solution is described in Appendix B. In the Keplerian solution of Fig. 11, the Rayleigh condition is violated over the whole region of the angular momentum deposition. Then, the minimum surface density is given by equation (B3), which is much larger than our solution and equation (41). Because equation (B3) does not satisfy equation (35), the Keplerian solution does not satisfy the angular momentum conservation, as pointed out in Section 4.3. On the other hand, in the zero-dimensional analysis by Fung et al. (2014, or in equation 41), s_{min} is estimated from a balance between the planetary torque and the viscous angular momentum flux (i.e. from the angular momentum conservation). Because of this difference, the Keplerian solution gives a much shallower gap than the estimation in equation (41). Note that because our exact solutions are given by equation (27), the balance between the planetary torque and the viscous angular momentum flux is always satisfied in our solutions. Hence, our solutions always satisfy the angular momentum conservation and gives a similar s_{min} to equation (41) for a sufficiently wide gap.

5.2 Dependences of the gap depth and width on *K*

Fig. 12 shows the minimum surface densities s_{min} as a function of the parameter K similar to Fig. 8 but the effect of the wave propagation is included in this figure. In this figure, we also show the dependence on the parameter x_d while w_d is fixed at h_p since w_d does not change the surface density distribution much (see Fig. 10). At $K = 200$, as also seen in Fig. 9, our exact solutions reproduce the gap depth of DM13 (or the wide-limit gap) for $x_d \geq 3$. At $K = 1000$, on the other hand, a larger x_d (≥ 6) is required for agreement with DM13. That is, with an increase of K, a large x_d is necessary for the values of the depth of the hydrodynamic simulations to agree. Note that the dashed lines in Fig. 12 represent the cases of unrealistic wave propagation, in which more than half of the one-sided torque is due to the excitation at $|x| > x_d$, as for the case of $x_d = 2$ in Fig. 9. At large K, a large x_d is also required for realistic wave propagation.

We also show the Keplerian solution with the wave propagation of $x_d = 6$ (see Appendix B). For $K > 30$, s_{min} is given by equation (B3) and independent of K because of the Rayleigh condition, as seen in Fig. 9. This unrealistic result in the Keplerian solution is related with the violation of the angular momentum conservation, as pointed out in Section 4.3 (and see also Appendix B). To check which x_d is preferable, we also compare the gap width with the hydrodynamic simulations. Fig. 13 shows the gap width of the exact solutions as a function of K. Similar to DM13, the gap edge is defined by the position with $s = 1/3$. In this definition, the gap width is roughly given by twice $x_d h$ for our exact solutions with $K > 50$. Note that this definition is useless for $K < 50$ because of shallow gaps with $s_{min} > 1/3$. The dashed lines represent the cases of unrealistic wave propagation, similar to Fig. 12. The results of DM13 and Varnière et al. (2004) are also plotted in fig. 13. Varnière et al. (2004) also performed hydrodynamic simulations of gap formation for $M_p/M_* = 10^4$–2×10^3, $\alpha = 6 \times 10^{-2}$–$6 \times 10^{-5}$ and $h_p/R_p = 0.04$ (i.e. $K = 600$–6×10^5). Their gap depths almost agree with DM13's relation. For $K < 300$, our exact solutions with $x_d = 3$ and 4 agree with the results of DM13 and Varnière et al. (2004), respectively. For $K > 300$, on the other hand, the widths obtained by Varnière et al. (2004) are wider than those given by DM13. Our exact solution with $x_d = 6$ agrees with the widths of Varnière et al. (2004), while widths of DM13 correspond to our

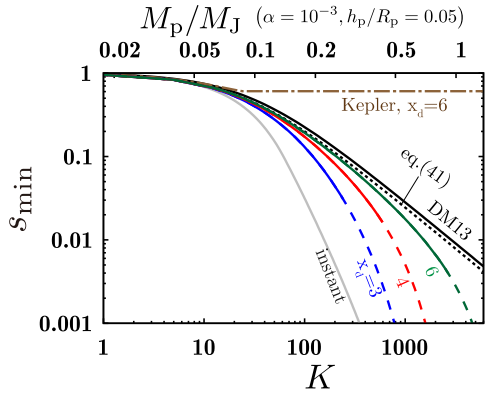

Figure 12. Minimum surface densities, s_{min}, of the exact solutions in the case with the wave propagation for $x_d = 3$ (blue), 4 (red) and 6 (green). The parameter w_d is h_p. We also plot results by DM13 (equation 42, solid line) and the wide-limit gap (equation 41, dotted line) and the exact solution with instantaneous damping (grey line). The dashed lines indicate exact solutions with unrealistic wave propagation.

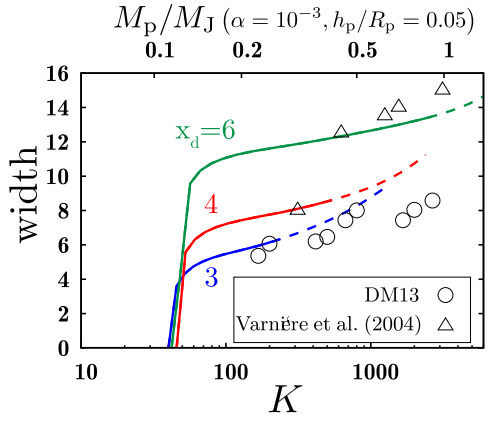

Figure 13. Gap widths of our solutions for $x_d = 3$ (blue), 4 (red) and 6 (green). The edge of the gap is defined by the position with $s = 1/3$, in the same way as defined by DM13. The parameter w_d is set to h_p. The dashed lines represent solutions with unrealistic wave propagation, similar to Fig. 12. The circles indicate the gap widths obtained by DM13 (fig. 6 of their paper), and the triangles show the gap widths by Varnière et al. (2004, twice Δ_{1000} in table 1 of Varnière et al.).

solutions of unrealistic wave propagation. The preferable x_d cannot be determined only by this comparison, and we still have a large uncertainty in the preferable value of x_d.

The difference of widths between DM13 and Varnière et al. (2004) would be caused by different parameters in their simulations (e.g. the disc viscosity, spatial resolution and width of a computation domain). However, the origin of the difference is still unclear. Note that the results of Kley & Dirksen (2006) and Fung et al. (2014) may support the wide gap formation of Varnière et al. (2004). Kley & Dirksen (2006) also showed that the disc rotation has some eccentricity when the gap is extended to the 1:2 Lindblad resonance. The eccentric gaps are formed for a large K ($\gtrsim 10^4$) (e.g. Kley & Dirksen 2006; Fung et al. 2014). Such wide gaps by massive giant planets are beyond the scope of our one-dimensional disc model adopting the local approximation.

In the above, we found that a larger x_d is required for a larger K (i.e. a massive planet) in order to reproduce the minimum surface densities derived by DM13 and Varnière et al. (2004). It should be noted that the propagation distance is not proportional to the parameter x_d. The propagating distance of waves is defined by the distance from the wave excitation site to the angular momentum deposition site (i.e. x_d). Since the one-sided torque is radially distributed (see Fig 9b), the wave excitation site can be approximately given by the median of the distribution, i.e. the point within the half of the one-sided torque arises. Such an excitation site shifts away from the planet with an increase of K (see Fig. 12).[4] D'Angelo & Lubow (2010) also showed this tendency that the peak of the excitation torque density shifts away from the planet as a deep gap is formed (fig. 15 in that paper), using hydrodynamic simulations. Hence, because of this shift of the excitation site, the propagating distance does not increase much as x_d with K. Goodman & Rafikov (2001) showed that the propagating distance of waves decreases with an increase of the planet mass due to the non-linear wave damping. Hence, further studies are needed in order to confirm whether this results given by Goodman & Rafikov (2001) conflicts with ours because of the shift of the excitation site. Furthermore, the non-linear wave damping would be weakened by the steep surface density gradient at the gap edge, as pointed out by Petrovich & Rafikov (2012). In order to fix the parameter x_d, such a wave damping effect in the gap should be taken into account in future work.

6 SUMMARY AND DISCUSSION

We re-examined the gap formation in viscous one-dimensional discs with a new formulation. In our formulation, we took into account the deviation from Keplerian disc rotation and included the Rayleigh stable condition, consistently. We also examined the effect of wave propagation. Our results are summarized as follows.

(i) The deviation from the Keplerian disc rotation makes the gap shallow. This is because of the enhancement of the shear motion and the viscous angular momentum transfer at the gap edges (see Fig. 4).

(ii) For deep gaps, the deviation from the Keplerian disc rotation is so large that the Rayleigh stable condition is violated. An enhanced viscosity dissolves such unstable rotation and makes it marginally stable (see Fig. 7). This effect also makes the gap shallower (see Fig. 6).

(iii) To include the effect of wave propagation, we adopted a simple model where the position of the angular momentum deposition is parametrized by x_d. A large x_d indicates a long propagation length. The effect of wave propagation makes the gap wider and shallower (Fig. 9). In a wide gap, the waves are mainly excited at the flat bottom, which reduces the one-sided torque and the gap depth. For a sufficiently large x_d, the gap depth of our exact solution agrees well with the wide-limit gap and with the results of hydrodynamic simulations. At $K = 1000$, our model requires $x_d \geq 6$ for the agreement (Fig. 12). In the case of instantaneous wave damping, on the other hand, our exact solution gives much deeper gaps than those of hydrostatic simulations.

(iv) To check the validity of the large x_d, the gap width of our exact solution is compared with results of hydrodynamic simulations. For $K = 1000$, our exact solution with $x_d \geq 6$ has a gap width of $12h_p$, which is larger than those of DM13 ($\sim 8h_p$). The gap widths of Varnière et al. (2004), on the other hand, are almost consistent with our exact solutions. Because of this uncertainty in the gap width of hydrodynamic simulations, it is difficult to fix the preferable x_d by this comparison.

(v) When the Rayleigh condition is taken into account, the deviation from the Keplerian rotation should also be included in order to keep the angular momentum conservation. The Keplerian solutions with the Rayleigh condition give much shallower gaps, as shown in Figs 8 and 12.

In future works, we need to determine the preferable value of x_d. Previous studies (e.g. Korycansky & Papaloizou 1996; Takeuchi, Miyama & Lin 1996; Goodman & Rafikov 2001; Dong, Rafikov & Stone 2011) have investigated the wave propagation with no gap. As pointed out by Petrovich & Rafikov (2012), however, the gap structure can affect the wave damping. Since our result shows that the wave damping significantly affects both the gap depth and width, the wave damping should be treated accurately in both one-dimensional models and hydrodynamic simulations for gap formation.

Our simple model does not include the effect of the deviation from Keplerian disc rotation on the wave excitation. Petrovich & Rafikov (2012) showed that a steep surface density gradient modifies the excitation torque. Such an effect on the wave excitation should be included in future studies on the gap formation. Nevertheless, it is also considered that when the waves are mainly excited at the flat-bottom, such as for the wide-limit gap, the deviation of the disc rotation would not affect the wave excitation significantly.

We also neglect the non-linearity of wave excitation, whereas the non-linearity cannot be neglected for large planets as $M_p/M_* \gtrsim (h_p/R_p)^3$. According to Miyoshi et al. (1999), the non-linearity makes the excitation torque small compared to the value for linear theory. This possibly leads to an additional shallowing effect. However, this effect would not significantly influence the gap depth since s_{min} is scaled by only K in DM13's relation (equation 42).

The Rossby wave instability may be essential for the gap formation. In the present study, we included only the Rayleigh condition. A more detail investigation including both the Rayleigh condition and the Rossby wave instability should be done in future works.

ACKNOWLEDGEMENTS

We are grateful to Aurélien Crida, and Alessandro Morbidelli for their valuable comments. We also thank the anonymous referee for useful comments on the manuscript. KDK is supported by Grants-in-Aid for Scientific Research (26103701) from the MEXT

[4] In Fig. 12, the exact solution have transition points from the realistic wave propagation (solid lines) to the unrealistic one (dashed lines) for each x_d. At the transition point of K, the excitation site defined by the median is equation to x_d. Fig. 12 shows that the excitation site moves away from the planet with an increasing K since the transition point of K increases with x_d.

of Japan. TT (Takayuki Tanigawa) is supported by Grants-in-Aid for Scientific Research (23740326 and 24103503) from the MEXT of Japan.

REFERENCES

Abramowitz M., Stegun I. A., 1965, Handbook of Mathematical Functions with Formulas, Graphs, and Mathematical Tables. Dover Press, New York
Adachi I., Hayashi C., Nakazawa K., 1976, Prog. Theor. Phys., 56, 1756
Artymowicz P., Lubow S. H., 1994, ApJ, 421, 651
Artymowicz P., Lubow S. H., 1996, ApJ, 467, L77
Bate M. R., Lubow S. H., Ogilvie G. I., Miller K. A., 2003, MNRAS, 341, 213
Chandrasekhar S., 1939, Ciel Terre, 55, 412
Chandrasekhar S., 1961, Hydrodynamic and Hydromagnetic Stability. Oxford Univ. Press, Oxford
Crida A., Morbidelli A., Masset F., 2006, Icarus, 181, 587
D'Angelo G., Lubow S. H., 2010, ApJ, 724, 730
D'Angelo G., Henning T., Kley W., 2002, A&A, 385, 647
Dodson-Robinson S. E., Salyk C., 2011, ApJ, 738, 131
Dong R., Rafikov R. R., Stone J. M., 2011, ApJ, 741, 57
Duffell P. C., MacFadyen A. I., 2013, ApJ, 769, 41 (DM13)
Fung J., Shi J.-M., Chiang E., 2014, ApJ, 782, 88
Goldreich P., Tremaine S., 1980, ApJ, 241, 425
Goodman J., Rafikov R. R., 2001, ApJ, 552, 793
Haisch K. E., Jr, Lada E. A., Lada C. J., 2001, ApJ, 553, L153
Kanagawa K. D., Fujimoto M. Y., 2013, ApJ, 765, 33
Kley W., 1999, MNRAS, 303, 696
Kley W., Dirksen G., 2006, A&A, 447, 369
Kokubo E., Ida S., 2000, Icarus, 143, 15
Kokubo E., Ida S., 2002, ApJ, 581, 666
Korycansky D. G., Papaloizou J. C. B., 1996, ApJS, 105, 181
Li H., Finn J. M., Lovelace R. V. E., Colgate S. A., 2000, ApJ, 533, 1023
Lin D. N. C., Papaloizou J., 1979, MNRAS, 186, 799
Lin D. N. C., Papaloizou J., 1986, ApJ, 309, 846
Lin D. N. C., Papaloizou J. C. B., 1993, in Levy E. H., Lunine J. I., eds, Protostars and Planets III. Univ. Arizona Press, Tucson, AZ, p. 749
Lin M.-K., 2014, MNRAS, 437, 575
Lubow S. H., D'Angelo G., 2006, ApJ, 641, 526
Lubow S. H., Seibert M., Artymowicz P., 1999, ApJ, 526, 1001
Lynden-Bell D., Pringle J. E., 1974, MNRAS, 168, 603
Miyoshi K., Takeuchi T., Tanaka H., Ida S., 1999, ApJ, 516, 451
Mizuno H., 1980, Prog. Theor. Phys., 64, 544
Muto T., Inutsuka S.-i. 2009, ApJ, 701, 18
Petrovich C., Rafikov R. R., 2012, ApJ, 758, 33
Rafikov R. R., 2002, ApJ, 572, 566
Richard S., Barge P., Le Dizès S., 2013, A&A, 559, A30
Shakura N. I., Sunyaev R. A., 1973, A&A, 24, 337
Takeuchi T., Miyama S. M., 1998, PASJ, 50, 141
Takeuchi T., Miyama S. M., Lin D. N. C., 1996, ApJ, 460, 832
Tanaka H., Takeuchi T., Ward W. R., 2002, ApJ, 565, 1257
Tanigawa T., Ikoma M., 2007, ApJ, 667, 557 (TI07)
Varnière P., Quillen A. C., Frank A., 2004, ApJ, 612, 1152
Ward W. R., 1986, Icarus, 67, 164
Ward W. R., 1997, Icarus, 126, 261
Yang C.-C., Menou K., 2010, MNRAS, 402, 2436
Zhu Z., Nelson R. P., Hartmann L., Espaillat C., Calvet N., 2011, ApJ, 729, 47
Zhu Z., Stone J. M., Rafikov R. R., 2013, ApJ, 768, 143

APPENDIX A: GAP MODEL BY TI07

Following TI07, we describe surface density structures of gap in a disc with the Keplerian rotation. In this section, we consider the gap structure in the case of instantaneous wave damping. The gap structure in the case with wave propagation is discussed in Appendix B. In the case of instantaneous wave damping, the angular momentum deposition rate is given by $\lambda_{\rm ex}$ given by equation (30). At far from a planet, the Rayleigh condition is always satisfied because the planetary gravity is weak. Hence, the gradient of surface density is given by equation (36) and the second derivative of surface density is given by

$$\frac{{\rm d}^2 \ln s}{{\rm d}x^2} = \mp \frac{4KC}{3x^5}. \tag{A1}$$

The stability of the Rayleigh condition is checked by equation (A1). Namely, when ${\rm d}^2 \ln s/{\rm d}x^2 < -1$ in equation (A1), the surface density is described by the marginal Rayleigh stable state, instead of equation (37). We should point out that the second derivative given by equation (A1) is used to determine the stability of the Rayleigh condition and does not affect the surface density distribution. Because of this, the surface density gradient is steeper and the shallowing effect of the Rayleigh condition is much higher than in our model. Using equation (30), we obtain the outer edge of the marginal Rayleigh stable region, $x = x_{\rm m}$, as

$$x_{\rm m} = \left(\frac{4}{3}CK\right)^{1/5}. \tag{A2}$$

In consideration of the continuity of the surface density distribution, the surface density in the marginal Rayleigh stable region ($x < x_{\rm m}$) is given by

$$\ln s = -\frac{5}{6}x_{\rm m}^2 + \frac{5}{4}x_{\rm m}|x| - \frac{1}{2}x^2, \tag{A3}$$

$$= -0.854K^{2/5} + 1.266K^{1/5}|x| - 0.5x^2, \tag{A4}$$

and the surface density for $x > x_{\rm m}$ is given by equation (37). Since there is no torque density for $x > 1.3$ in this case, the minimum surface density $s_{\rm min}$ is given by $s(x = 1.3)$. Thus, we give $s_{\rm min}$ as

$$s_{\rm min} = \exp\left(-0.854K^{2/5} + 1.645K^{1/5} - 0.845\right). \tag{A5}$$

Note that if $x_{\rm m} < 1.3$, the whole region of the gap is the Keplerian rotating part and $s_{\rm min}$ is given by equation (37) with $x = 1.3$. It should be also noticed that the angular momentum conservation is not satisfied at the flat-bottom region with $s = s_{\rm min}$ of equation (A5), as explained in the subsection 4.3 (and see also, Appendix B).

APPENDIX B: GAP MODEL IN A KEPLERIAN ROTATING DISC WITH WAVE PROPAGATION

Here, by assuming the Keplerian disc rotation, we derive gap solutions in the case with wave propagation. Following TI07, we consider the marginal condition when the Rayleigh condition is violated. The angular momentum deposition rate is given by equation (32). Ignoring deviation in ${\rm d}\Omega/{\rm d}R$ form the Keplerian and differentiating, we give

$$\frac{{\rm d}s}{{\rm d}x} = \begin{cases} \dfrac{\bar{T}}{3}\dfrac{h_{\rm p}}{w_{\rm d}} & \text{for } x_{\rm d} - \dfrac{w_{\rm d}}{2h_{\rm p}} < |x| < x_{\rm d} + \dfrac{w_{\rm d}}{2h_{\rm p}}, \\ 0 & \text{otherwise.} \end{cases} \tag{B1}$$

Integrating equation (B1), we obtain the surface density without the Rayleigh condition as

$$s = \begin{cases} 1 & \text{for } |x| > x_{\rm d} + \frac{w_{\rm d}}{2h_{\rm p}}, \\ 1 - \frac{\bar{T}h_{\rm p}}{3w_{\rm d}}\left[\left(x_{\rm d} + \frac{w_{\rm d}}{2h_{\rm p}}\right) - x\right] & \text{for } x_{\rm d} - \frac{w_{\rm d}}{2h_{\rm p}} < |x| < x_{\rm d} + \frac{w_{\rm d}}{2h_{\rm p}}, \\ 1 - \frac{\bar{T}}{3} & \text{for } |x| < x_{\rm d} - \frac{w_{\rm d}}{2h_{\rm p}}. \end{cases} \tag{B2}$$

Equation (B2) does not satisfy the Rayleigh condition, especially for a large K (or a large $\tilde{T}$). First, the Rayleigh condition is violated near $|x| = x_{\rm d} + w_{\rm d}/2h_{\rm p}$ because ${\rm d}s/{\rm d}x$ of equation (B1) is not continuous there. In order to make ${\rm d}s/{\rm d}x$ continuous, the marginally stable condition (equation 29) is used instead of equation (B1) in the region where $x_{\rm d} + w_{\rm d} - (\tilde{T}h_{\rm p})/(3w_{\rm d}) < |x| < x_{\rm d} + w_{\rm d}/2h_{\rm p}$. In addition, the marginally stable condition should also be used near $|x| = x_{\rm d} - w_{\rm d}/2h_{\rm p}$ for a large $\tilde{T}$. From equation (B1), we find that the Rayleigh condition is violated from $|x| = x_{\rm d} - w_{\rm d}/2h_{\rm p}$ to $x_{\rm d} + (w_{\rm d}/2h_{\rm p})(1 - 6/\tilde{T}) + 1$. These two Rayleigh unstable regions are merged for $\tilde{T} > 3(w_{\rm d}/h_{\rm p})$. In such large-$K$ cases, since the marginally stable condition is used in the whole region of the angular momentum deposition, the minimum surface density is given by

$$s_{\rm min} = \exp\left[-\left(\frac{1}{2} + \frac{h_{\rm p}}{w_{\rm d}}\right)\right] \tag{B3}$$

which is independent of K. This unrealistic minimum surface density does not satisfy equation (35) which is originated by the angular momentum conservation. As indicated by Fung et al. (2014), the planetary torque should balance with the viscous angular momentum flux outside the gap for the angular momentum conservation. In our formulation, two terms in the right-hand side of equation (27) balance with each other in the bottom region (the left-hand side is negligibly small). However, the minimum surface density given by equation (B3) independent of K breaks down such a balance. Hence, equation (B3) also violates the angular momentum conservation.

For a small K, equation (B2) is approximately valid because the Rayleigh unstable region near $|x| = x_{\rm d} + w_{\rm d}/2h_{\rm p}$ does not significantly affect $s_{\rm min}$. Substituting equation (B2) into equation (33), we give $\tilde{T}$ as

$$\tilde{T} = 3\left[\frac{9\Delta^3}{KC}\left(1 - \frac{KCx_{\rm d}}{9\left[x_{\rm d}^2 - (w_{\rm d}/2h_{\rm p})^2\right]^2}\right) + 1\right]^{-1}. \tag{B4}$$

Substituting equation (B2) into equation (B4), we obtain $s_{\rm min}$ for a small K as

$$s_{\rm min} = \left[\frac{CK}{9\Delta^3}\left(1 - \frac{KCx_{\rm d}}{9\left[x_{\rm d}^2 - (w_{\rm d}/2h_{\rm p})^2\right]^2}\right)^{-1} + 1\right]^{-1}. \tag{B5}$$

APPENDIX C: SOLUTIONS FOR THE LINEARIZED EQUATION OF GAPS

Here, we consider solutions to the following differential equation:

$$\frac{{\rm d}^2 y}{{\rm d}x^2} - 3y = g(x), \tag{C1}$$

where $g(x)$ is an arbitrary odd function of x. A general solution of this equation is given by a combination of homogeneous solutions, $e^{\pm\sqrt{3}x}$, and a particular solution. We seek a solution which satisfies the boundary conditions of $y = 0$ at $x = \pm\infty$. Since $g(x)$ is odd in this case, the solution is an even function of x. For simplicity, we consider the solution for $x > 0$. Because of the symmetry of the equation, the solution of $x < 0$ can be obtained by inverting the sign of x in the solution for $x > 0$.

A particular solution $y_{\rm p}(x)$ of equation (C1) can be given by

$$y_{\rm p}(x) = \frac{1}{2\sqrt{3}}\left[e^{\sqrt{3}x}\int_x^\infty g(x')e^{-\sqrt{3}x'}{\rm d}x' - e^{-\sqrt{3}x}\int_x^\infty g(x')e^{\sqrt{3}x'}{\rm d}x'\right]. \tag{C2}$$

In the case with instantaneous wave damping (see equation 44), $g(x)$ is given by

$$g(x) = -\begin{cases} \dfrac{C}{3|x|^3} & \text{for } |x| > \Delta, \\ \dfrac{C}{3\Delta^3} & \text{otherwise.} \end{cases} \tag{C3}$$

Substituting equation (C3) into equation (C2), the particular solution for $x > \Delta$ is obtained as

$$y_{\rm p}(x) = \frac{\sqrt{3}C}{18}\left[-\frac{\sqrt{3}}{x} + \frac{3}{2}\left\{e^{-\sqrt{3}x}Ei(\sqrt{3}x) - e^{\sqrt{3}x}Ei(-\sqrt{3}x)\right\}\right], \tag{C4}$$

where $Ei(ax)$ denotes the exponential integral function (e.g. Abramowitz & Stegun 1965). For $x \leq \Delta$, the particular solution is given by

$$y_{\rm p}(x) = a_+ e^{\sqrt{3}x} + a_- e^{-\sqrt{3}x} + \frac{C}{9\Delta^3}, \tag{C5}$$

where a_+ and a_- are defined by

$$a_\pm = \frac{C}{6}\left[\mp Ei(\mp\sqrt{3}\Delta) - \frac{1}{\Delta}\left(\frac{1}{3\Delta^2} + \frac{1}{2}\right)e^{\mp\sqrt{3}\Delta}\right]. \tag{C6}$$

Using this particular solution given by equations (C4) and (C5), we can obtain the general solution of equation (44). Since this particular solution vanishes at $x \to \infty$, the coefficient of the homogeneous solution $e^{\sqrt{3}x}$ is zero. The coefficient of $e^{-\sqrt{3}x}$, B, is obtained as

$$B = \frac{1}{\sqrt{3}}\left.\frac{{\rm d}y_{\rm p}}{{\rm d}x}\right|_{x=0}. \tag{C7}$$

This paper has been typeset from a TEX/LATEX file prepared by the author.